Control of Common Resonances in Bichromatically Driven Hydrogen Atoms

Leszek Sirko[1,2] and Peter M. Koch[1]

[1]*Department of Physics and Astronomy, State University of New York, Stony Brook, New York 11794-3800*
[2]*Institute of Physics, Polish Academy of Sciences, Aleja Lotników 32/46, 02-668 Warszawa, Poland*

(Received 7 June 2001; revised manuscript received 24 April 2002; published 16 December 2002)

We report the first combined experimental-theoretical study to realize and control the behavior of common resonances in a periodically driven system. Experimental data for the ionization of H($n = 51$) atoms by a bichromatic (6 and 18 GHz), linearly polarized electric field pulse show how the relative field phase can be used to control the ionization. 1D classical calculations show how this results from the phase control of the pendulumlike, common resonances, whose existence requires, at lowest order, two commensurate frequencies.

DOI: 10.1103/PhysRevLett.89.274101 PACS numbers: 05.45.Gg, 05.45.Mt, 32.80.Qk, 32.80.Rm

The distinctive feature of Hamiltonian, nonintegrable classical dynamics is nonlinear resonance [1]. Manipulation of resonance parameters allows one to control nonlinear systems. Physics and engineering give many macroscopic examples of such situations, ranging from particles in storage rings and plasmas to electronic and mechanical devices. The study of microscopic systems raises the additional question of quantal-classical correspondence. Understanding when and how correspondence does or does not occur if classical chaos is involved is a key issue in quantum chaos studies [2].

A linear system driven at its resonant frequency must continue to absorb energy. A nonlinear system is different. Consider an undamped pendulum subject to gravity. Small amplitude librations have a period T fixed at the linear-resonance value, $T_r = 2\pi/\omega_r$. With increasing amplitude, T increases, diverging logarithmically on the *separatrix* (inverted pendulum) between bounded librational motion and unbounded, rotational motion. To put more energy into a librating pendulum driven at frequency $\omega = \omega_r$ requires either increasing the drive, decreasing ω, or both. This is the most elementary control of a nonlinear resonance.

When a more complicated nonlinear Hamiltonian system is periodically driven, a periodic sampling of its orbits (Poincaré section) generally shows many nonlinear resonances. The example used in this Letter is the periodically forced, 1D hydrogen atom [3]. In atomic units (qv, [4], p. 292) its Hamiltonian is $\mathcal{H}(x, p, t) = p^2/2 + V(x) + \lambda(t)xF(t)$, where $V(x > 0) = -1/x$, $V(x \leq 0) = \infty$, $F(t + \tau) = F(t)$ is a periodic electric field, and $\lambda(t)$ is an envelope function. Each of its nonlinear resonances has different pendulum parameters. Deterministic chaos occurs first near separatrices. Increasing the driving increases of the width of resonance zones and their surrounding chaotic layers until overlapping of neighboring resonances leads to global chaos and the onset of ionization of the classical atom. The resonance overlap criterion introduced by Chirikov [5] gives a quantitative, classical estimate for the ionization threshold field [1,3,4,6].

The general description of quantal nonlinear resonance is known [7], and some details of the quantal-classical correspondence have been worked out for the driven 1D [8] and 3D [9] H atom. Comparisons [4] of a large body of experimental data with the results of classical and quantal calculations have shown where to expect quantal-classical correspondence in the ionization behavior. The most important parameter is the scaled frequency $n^3\omega \equiv \Omega$, which quantally (classically) is ω over the $\Delta n = 1$ frequency splitting for principal quantum number $n \gg 1$ (over the Kepler frequency ω_k). When $\Omega \gtrsim 2$, quantal effects such as dynamical localization raise quantal ionization thresholds above classical values [10–12]. For lower values of Ω, one usually finds good quantal-classical agreement until Ω gets so low that the ionization mechanism becomes quasistatic: quantal tunneling through (classical escape over) the Coulomb-Stark potential barrier [13]. We are concerned here with $\Omega \geq 0.12$, where the ionization mechanism is not quasistatic [14].

We report in this Letter the first, combined experimental, numerical, and approximate analytical study to realize and control the behavior of nonlinear *common resonances* (CR), so named [15] because they require both driving frequencies. What we call *independent resonances* (IR) are different; IR remain when one or the other of the two bichromatic field amplitudes is zero. We realize CRs with excited H atoms driven by a linearly polarized electric field consisting of two commensurate frequencies (2f). We show how the relative field phase can be used to affect the details of CRs and, thereby, to control the ionization probability. Our comparisons between experiment and calculations show excellent quantal-classical correspondence near the onset of ionization.

Our experiment uses a 14.6 keV beam of $n = 51$ H atoms. Laser excitation of the atoms occurs in a static electric field and raises them to an individual quantal substate, but subsequent stray-field-induced transitions cause atoms to arrive at the microwave interaction region with a nearly uniform distribution of substates in the $n = 51$ manifold [4]. Because this corresponds to a

microcanonical ensemble of classical orbits in three spatial dimensions, our experiment uses "3D atoms."

The H atoms cross a linearly polarized, microwave field traveling in a WRD-500 double-ridge waveguide; atoms enter and exit via 0.25 mm holes drilled in opposing sidewalls. The waveguide operates single mode from below 4.5 to above 18 GHz, and each atom sees the spatial variation of the mode as an envelope $0 \leq \lambda(t) \leq 1$ that slowly modulates the peak electric amplitude F. The inset in Fig. 1 shows the first half of $\lambda(t)$, which is symmetric about $t = 0$. To compare time scales, its 2 ns flat top lasts about 100 Kepler periods of an $n = 51$ electron and 12 field oscillations, say, of $\omega/2\pi = 6$ GHz.

Generation of the 2f field begins with a comb generator that produces harmonics of a synthesized 1 GHz signal. A divider splits the comb-generator output, and a tunable filter in each arm selects the desired harmonic. After amplification and suppression of broadband amplifier noise with filters, the harmonics are combined and injected into the waveguide. Hereafter, we use subscripts on ω and F as follows: α and β denote unspecified frequencies; a number gives a specific frequency in GHz. The bichromatic field is $F_{\rm bi}(t) = [F_\alpha \sin(\omega_\alpha t') + F_\beta \sin(\omega_\beta t' + \phi)]$, with $\omega_\alpha > \omega_\beta$ and $t' = t + t_0$. We verify stability of ϕ at the few degree level and calibrate the F_α and F_β scales to 5% [16]. Because atoms enter the field at random times t_0, the experiment averages the phase between the electron motion and field oscillation [17].

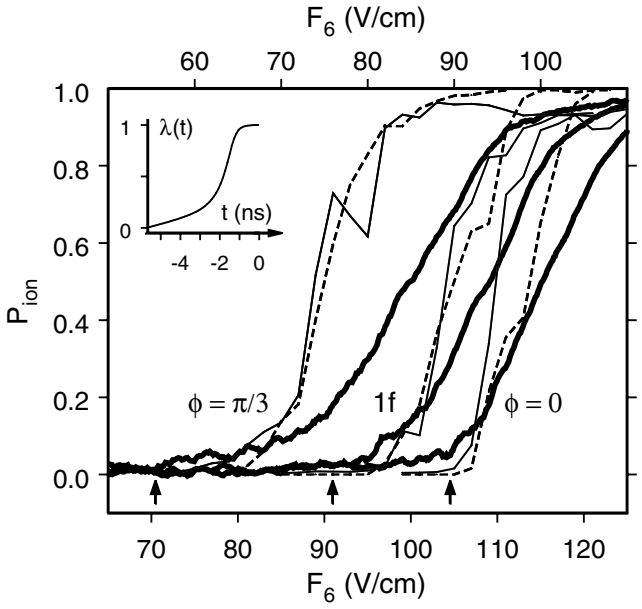

FIG. 1. Ionization curves for $n = 51$ H atoms. Thick lines: experiment with 3D atoms. Thin solid (dashed) lines: quantal (classical) 1D calculations. Thick (thin) curves use the lower (upper) F_6 scale for 6 GHz peak field amplitude. One-frequency (1f) results are for the 6 GHz field alone. Two-frequency (2f) results are with an 18 GHz field added, with $F_{18} = 6$ V/cm, for relative phase $\phi = \pi/3$ (leftmost group) and $\phi = 0$ (rightmost group). Arrows: resonance-overlap estimates for onset of global chaos for the two 2f cases and one 1f case. Inset: First half of the envelope function $\lambda(t)$ for the microwave amplitude; it is symmetric about $t = 0$.

The three thick curves in Fig. 1 show measured ionization probability [18] $P_{\rm ion}$ vs F_6 for 3D H($n = 51$) atoms. For two different values of ϕ, the 2f curves in Fig. 1 show $P_{\rm ion}$ vs F_6 when an 18 GHz field with $F_{18} = 6$ V/cm is present. Between them lies the 1f curve obtained with 6 GHz alone, i.e., with $F_{18} = 0$. Let us focus on 10% thresholds, viz., where $P_{\rm ion}$ first crosses 0.1: the 1f value is about 96 V/cm; the 2f values are, respectively, about 107 V/cm for $\phi = 0$ and 85 V/cm for $\phi = \pi/3$. Figure 1 clearly demonstrates that changing ϕ exerts significant control over the 2f ionization.

We need to explain this behavior. For a 1:3 frequency ratio, the peak 2f-field amplitude minimizes at $|F_6 - F_{18}|$ for $\phi = 0$ and maximizes at $(F_6 + F_{18})$ for $\phi = \pi/3$. The phase dependence would be trivially explained if the onset of ionization were determined entirely by the peak 2f-field amplitude, as would occur for the quasistatic case mentioned earlier [13,14]. Here, relative to the 1f 10% threshold, about 96 V/cm, and F_{18} fixed at 6 V/cm, trivial behavior would be a 10% threshold of $96 + 6 = 102$ V/cm for $\phi = 0$ and $96 - 6 = 90$ V/cm for $\phi = \pi/3$. That the actual 10% thresholds, about 107 and 85 V/cm, respectively, are significantly above and below these values stimulates a dynamical explanation for the nontrivial phase dependence.

The six thin curves in Fig. 1 come from calculations using $\mathcal{H}(x, p, t)$ with $F_{\rm bi}(t)$ and the experimental $\lambda(t)$. To simulate the experiment, we average the calculations over t_0 but fix the relative field phase ϕ. The three, thin, solid (quantal 1D: q1D) curves come from our numerical integrations of the time-dependent Schrödinger equation on a 1D, bound basis $n \in [35, 220]$. We define $P_{\rm ion}$ to be the fraction of population rising to n values above the cutoff $n_c = 130$, the same as in the experiment [18]. The three, thin, dashed (classical 1D: c1D) curves come from our Monte Carlo integrations of Hamilton's equations [19]. $P_{\rm ion}$ is defined to be the fraction of orbits rising to classical action $I > I_c = n_c$.

Previous work has shown why a 1D model explains the *onset* of ionization of 3D H atoms by linearly polarized microwaves: the driving field elongates 3D atoms along the polarization axis, allowing the driven electron to find the 1D escape route to ionization [3]. However, direct comparison of 1D calculations with 3D data requires care. The driving field supplies the energy leading to ionization when the electron passes near the proton. Because all 1D bound orbits hit the nucleus, whereas most 3D orbits do not, in the 1D model ionization curves rise more rapidly and ionization thresholds are lower [20].

To offset this systematic difference and facilitate 1D-3D comparisons, we shift the upper F_6 axis by 15 V/cm and use it for calculated 1D curves. The lower F_6 axis is used for the experimental 3D curves. Note that *field differences are the same for both scales, and we make 1D-3D comparisons only near the onset of ionization.*

That the q1D and c1D calculations agree and reproduce the shifts of experimental 10% thresholds is a striking example of quantal-classical correspondence that will justify our using a 1D classical model to demonstrate how the behavior of CRs explains the observed 2f phase dependence. First, we show in Fig. 2 Poincaré sections of orbits of $\mathcal{H}(x, p, t)$ at field amplitudes well below the onset of global chaos. IRs occur when $\omega{:}\omega_k = j{:}m$, where j, m are positive integers. In Fig. 2(a), calculated for $F_6 = 30\,\mathrm{V/cm}$ and $F_{18} = 0$, IR1 at $\omega{:}\omega_k = 1{:}8$ is too thin to be seen, and IR2 at 1:7 is barely evident. In Fig. 2(b), calculated for $F_{18} = 6\,\mathrm{V/cm}$ and $F_6 = 0$, IR1 at $\omega{:}\omega_k =$ 3:8 and IR2 at 3:7 are both too thin to be seen. [The degeneracy in action n of IRs in Figs. 2(a) and 2(b) occurs because $\omega_\alpha = 3\omega_\beta$.] Conversely, both fields together give significant common resonances; Fig. 2(c) [2(d)] shows CR1 and CR2 for $F_6 = 30\,\mathrm{V/cm}$ for $\phi = 0$ [for $\phi = \pi/3$].

2f driving gives more parameters to vary to control resonance overlap at higher field amplitudes. The simplest scenario, investigated for plasmas in [21] and H atoms in [15,22], uses a choice of ω_β that puts one of its IRs midway between two IRs of ω_α. But here we stress the role of CRs, which require, at lowest order, both driving frequencies; they occur at resonant values of action $n_r = \Omega^{-1/3}$ such that

$$j\Omega = \sigma_\alpha m_\alpha \omega_\alpha + \sigma_\beta m_\beta \omega_\beta, \tag{1}$$

where $j - 1, m_\alpha, m_\beta$ are non-negative integers and $\sigma_\alpha, \sigma_\beta = \pm 1$. We show next how the CRs in Figs. 2(c) and 2(d) affect the ionization dynamics with the stronger driving of Fig. 3 and that this explains the experimental results and calculations in Fig. 1.

We approximate the time-dependent Hamiltonian near a CR by a time-independent resonance Hamiltonian whose complicated form is worth examining:

$$\mathcal{H}_r = -\frac{3}{2}\frac{X^2}{n_r^4} + \sum_{\sigma_\alpha}\sum_{\sigma_\beta}\sum_{\eta=\alpha,\beta} H_\eta^{\sigma_\alpha\sigma_\beta}, \tag{2}$$

$$H_\eta^{\sigma_\alpha\sigma_\beta} = \sigma_\eta \frac{2}{3} n_r \omega_\eta \sum_j \frac{x_j}{j} \sum_{m_\alpha}\sum_{m_\beta} J_{m_\alpha}(ja_\alpha) J_{m_\beta}(ja_\beta) m_\eta \sin\gamma, \tag{3}$$

$$\gamma = j(\theta + a_\alpha + a_\beta\cos\phi) - \sigma_\beta m_\beta \phi - (m_\alpha + m_\beta - 1)\tfrac{\pi}{2}, \tag{4}$$

subject to the constraint, Eq. (1). In Eqs. (2)–(4), ϕ is the relative phase defined earlier; θ and $X = (n - n_r)$ are angle and action variables, respectively; J is an ordinary Bessel function and J' its derivative; $x_j = j^{-1}J_j'(j)$; $a_{\alpha,\beta} = 3n_r F_{\alpha,\beta}/\omega_{\alpha,\beta}$.

We need resonance widths $\mathcal{W}$ to use Chirikov's overlap criterion [1,5], but unless there is classical-quantal correspondence, the classical estimate is of little use to the experiment. A semiclassical estimate of the number of quantal states lying within a resonance is $\mathcal{A}/h$, where $\mathcal{A}$ is the area within the separatrix and h is Planck's constant. Because the jury is still out (see Table 2 in [4]) on the general question of how small (large) $\mathcal{A}/h$ must be for there to be quantal (classical) behavior, specific experimental/theoretical comparisons are needed and useful.

Though for 1f resonances, $j\Omega = m\omega$, $\mathcal{W}$ and $\mathcal{A}$ both grow as $F^{m/2}$ up to ionizing amplitudes [23], this is *not* the case for CRs. Which terms in the double sums over Bessel functions in Eq. (3) contribute most to a CR's growth depends on values of parameters; we find that neither $\mathcal{W}$ nor $\mathcal{A}$ of a CR need increase monotonically with amplitude(s).

It helps to consider specific examples. For $F_{18} = 6\,\mathrm{V/cm}$ and variable F_6, the double sums for CR1 are dominated by indices $(j, \sigma_\alpha m_\alpha, \sigma_\beta m_\beta) = (1, 0, 7), (1, 1, 4)$, and $(1, 2, 1)$. At the onset of ionization $\mathcal{A}/h$ for CR1 is about 2.1 for both $\phi = \pi/3$ (at $F_6 = 70.5\,\mathrm{V/cm}$) and

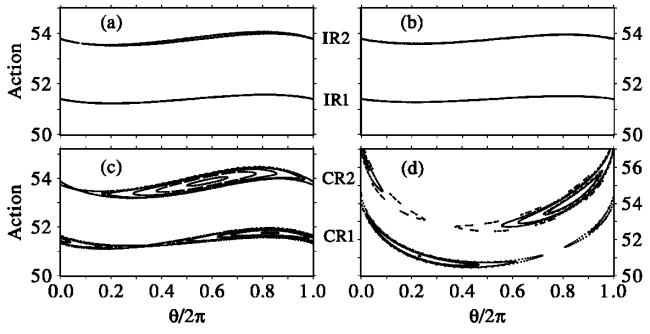

FIG. 2. Computed Poincaré sections of some 1D H atom orbits. CR1,CR2 (IR1,IR2) label common (independent) nonlinear resonances; see the text. (a) 6 GHz field with $F_6 =$ 30 V/cm. (b) 18 GHz field with $F_{18} = 6$ V/cm. (c),(d) 6 GHz field with $F_6 = 30$ V/cm and 18 GHz field with $F_{18} = 6$ V/cm both present, for relative phase $\phi = 0$ (c) and $\phi = \pi/3$ (d).

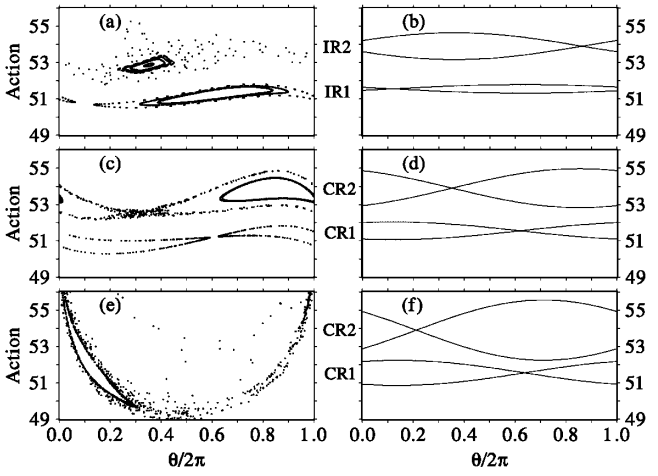

FIG. 3. Computed Poincaré sections (a),(c),(e) and analytical separatrices (b),(d),(f); see the text. In (a),(b) $F_6 = 70.5$ V/cm and $F_{18} = 0$; IR1 and IR2 do not overlap. In (c)–(f) $F_6 =$ 70.5 V/cm and $F_{18} = 6$ V/cm; Eqs. (2)–(4) give analytical separatrices for CR1 and CR2. In (c),(d) $\phi = 0$; CR1 and CR2 do not overlap. In (e),(f) $\phi = \pi/3$; CR1 and CR2 overlap.

$\phi = 0$ (at $F_6 = 104.5$ V/cm). The double sums for CR2 are dominated by $(j, \sigma_\alpha m_\alpha, \sigma_\beta m_\beta) = (1, 0, 8), (1, 1, 5)$, and $(1, 2, 2)$. At the onset of ionization $\mathcal{A}/h$ for CR2 is just below 0.9 for both $\phi = \pi/3$ ($F_6 = 70.5$ V/cm) and $\phi = 0$ (at $F_6 = 104.5$ V/cm); but $\mathcal{A}/h$ is significantly *higher*, viz., 1.4, for *smaller,* nonionizing values of F_6 (e.g., for $\phi = 0$ and $F_6 = 90$ V/cm).

With such small values of $\mathcal{A}/h$, no more than about two, it is surprising that the ionization mediated by these CRs exhibits such a fine quantal-classical correspondence. For $F_6 = 70.5$ V/cm, Figs. 3(c) and 3(e) show computed Poincaré sections for CR1 and CR2 [cf. Figs. 2(c) and 2(d)]; Figs. 3(d) and 3(f) show analytical separatrices found numerically from Eqs. (2)–(4). Note that though Poincaré sections with no external driving(not shown) give horizontal lines (action = constant), nonzero driving "bends" them, particularly so for $\phi = \pi/3$ in Figs. 2(d) and 3(e). Because our analytical model ignores all but the considered resonances, viz., IR1 and IR2 or CR1 and CR2, respectively, the separatrices in Figs. 3(b), 3(d), and 3(f) are not bent.

For the 1f case with $F_{18} = 0$, that computed orbits near $n = 51$ in Fig. 3(a) are not chaotic is consistent with the lack of overlap of IR1 and IR2 in Fig. 3(b). (The chaos near $n = 53$ occurs because IR2 overlaps with higher resonances, not shown here.) For the 2f case with $F_{18} = 6$ V/cm and $\phi = 0$, that computed orbits near $n = 51$ in Fig. 3(c) are not chaotic is consistent with lack of overlap of CR1 and CR2 in Fig. 3(d). For the 2f case with $F_{18} = 6$ V/cm and $\phi = \pi/3$, that global chaos in Fig. 3(e) "wipes out" CR2 and reaches down to CR1 is consistent with the overlap of CR1 and CR2 in Fig. 3(f).

For the data in Fig. 1, the results in Fig. 3 give a neat classical explanation for the onset of ionization for $\phi = \pi/3$ and for the lack of ionization at these field amplitudes for $\phi = 0$ and the 1f case. Arrows in Fig. 1 indicate the values of F_6 needed for resonance overlap. That each arrow in Fig. 1 is near the corresponding onset of ionization provides strong support for the classical interpretation we present in this Letter.

In summary, we use CRs to control microwave ionization of hydrogen atoms by a phase-locked, bichromatic field. We believe this is the first experimental realization and application of CRs. Given the theoretical existence of CRs elsewhere, e.g., in plasma wave heating [21], we expect that they will be useful for control of a wide variety of bichromatically driven systems.

NSF and ONR(DURIP) supported this work. L. S. acknowledges partial support from European Commission Contract No. ICA1-CT-2000-70018 and KBN Grant No. 2 P03B 023 17. S. Zelazny built the 2f microwave system.

[1] Entry points into an enormous literature include R. Z. Sagdeev, D. A. Usikov, and G. M. Zaslavsky, *Nonlinear Physics* (Harwood, Chur, Switzerland, 1988); A. J. Lichtenberg and M. A. Lieberman, *Regular and Chaotic Dynamics* (Springer, New York, 1992), 2nd ed.; L. E. Reichl, *The Transition to Chaos* (Springer, New York, 1992); R. Blümel and W. P. Reinhardt, *Chaos in Atomic Physics* (Cambridge University, Cambridge, 1997).
[2] G. Casati and B. Chirikov, *Quantum Chaos* (Cambridge University, Cambridge, 1995).
[3] M. M. Sanders and R.V. Jensen, Am. J. Phys. **64**, 21 (1996), and references therein.
[4] P. M. Koch and K. A. H. van Leeuwen, Phys. Rep. **255**, 289 (1995).
[5] B.V. Chirikov, Phys. Rep. **52**, 263 (1979). For recent work using the renormalization map to refine the Chirikov resonance overlap criterion, see C. Chandre, D. Farrelly, and T. Uzer, Phys. Rev. A **65**, 053402 (2002), and references therein.
[6] B. I. Meerson, E. A. Oks, and P.V. Sasorov, Pis'ma Zh. Eksp. Teor. Fiz. **29**, 79 (1979) [Sov. Phys. JETP Lett. **29**, 72 (1979)].
[7] G. P. Berman and G. M. Zaslavsky, Phys. Lett. **61A**, 295 (1977).
[8] L. Sirko and P. M. Koch, Appl. Phys. B **60**, S195 (1995).
[9] A. Buchleitner *et al.*, Eur. Phys. J. D **5**, 145 (1999).
[10] G. Casati, I. Guarneri, and D. L. Shepelyansky, Physica (Amsterdam) **163A**, 205 (1990), and references therein.
[11] E. J. Galvez *et al.*, Phys. Rev. Lett. **61**, 2011 (1988).
[12] J. E. Bayfield *et al.*, Phys. Rev. Lett. **63**, 364 (1989).
[13] B. E. Sauer *et al.*, , Phys. Rev. Lett. **68**, 468 (1992).
[14] We do not expect quasistatic behavior because the coupling constant presented in P. A. Dando and D. Richards, J. Phys. B **26**, 3001 (1993), C_n, is not much less than 1; see Sec. 3.5 of [4]. For $n = 51$ and $\omega/(2\pi) = 6$ GHz, $\Omega = 0.121$. At the 1f, 6 GHz, 10% threshold of 96 V/cm in Fig. 1, or $n^4F(10\%) = 0.126$, we get $C_n = 1.2$.
[15] J. E. Howard, Phys. Lett. A **156**, 286 (1991) named common resonances, showed they exist for driven, 1D H atoms, but did not investigate them further.
[16] L. Sirko, S. A. Zelazny, and P. M. Koch, Phys. Rev. Lett. **87**, 043002 (2001).
[17] M.W. Noel, L. Ko, and T. F. Gallagher, Phys. Rev. Lett. **87**, 043001 (2001) show that the phase between the electron motion and field oscillation can be used to control the 1f microwave ionization of Li Rydberg wave packets near pendulumlike resonances.
[18] The experimental n cutoff $n_c \simeq 130$; see Sec. 2.3.3 of [4].
[19] J. G. Leopold and I. C. Percival, Phys. Rev. Lett. **41**, 944 (1978).
[20] Compare 1D and 3D calculations in Figs. 9c and 10 in [4].
[21] J. E. Howard, A. J. Lichtenberg, and M. A. Lieberman, Physica (Amsterdam) **5D**, 243 (1982).
[22] A. Haffmans *et al.*, Phys. Rev. Lett. **73**, 248 (1994).
[23] R. Blümel, Phys. Rev. A **49**, 4787 (1994).